THE JOURNAL OF PHYSICAL CHEMISTRY B

pubs.acs.org/JPCB Article

Disassembly Intermediates of the Brome Mosaic Virus Identified by Charge Detection Mass Spectrometry

Kevin M. Bond,[†] Nicholas A. Lyktey,[†] Irina B. Tsvetkova, Bogdan Dragnea,* and Martin F. Jarrold*

Cite This: *J. Phys. Chem. B* 2020, 124, 2124–2131 Read Online

ACCESS | Metrics & More | Article Recommendations | Supporting Information

ABSTRACT: Capsid disassembly and genome release are critical steps in the lifecycle of a virus. However, their mechanisms are poorly understood, both in vivo and in vitro. Here, we have identified two in vitro disassembly pathways of the brome mosaic virus (BMV) by charge detection mass spectrometry and transmission electron microscopy. When subjected to a pH jump to a basic environment at low ionic strength, protein−RNA interactions are disrupted. Under these conditions, BMV appears to disassemble mainly through a global cleavage event into two main fragments: a near complete capsid that has released the RNA and the released RNA complexed to a small number of the capsid proteins. Upon slow buffer exchange to remove divalent cations at neutral pH, capsid protein interactions are disrupted. The BMV virions swell but there is no measurable loss of the RNA. Some of the virions break into small fragments, leading to an increase in the abundance of species with masses less than 1 MDa. The peak attributed to the BMV virion shifts to a higher mass with time. The mass increase is attributed to additional capsid proteins associating with the disrupted capsid protein−RNA complex, where the RNA is presumably partially exposed. It is likely that this pathway is more closely related to how the capsid disassembles in vivo, as it offers the advantage of protecting the RNA with the capsid protein until translation begins.

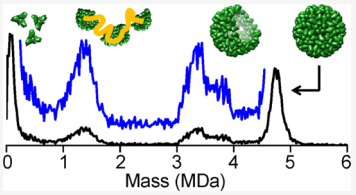

INTRODUCTION

Nonenveloped positive-sense single-stranded RNA (ssRNA) viruses[1] can be found in all domains of life and include many serious human pathogens. As there are few effective vaccines and antiviral drugs, new control methods are needed. RNA uncoating and its presentation to the host's translational machinery are crucial stages in the virus life-cycle. The genome of ssRNA viruses is protected by a capsid assembled from protein subunits. The capsid is a metastable structure: although it protects the genome outside the cell, it must be readily disrupted to present the genome for replication once inside.[2] Uncoating is regulated, temporally and spatially, in ways that are poorly understood, so that viral RNA is delivered intact to the right place and its presence does not trigger the defense mechanisms of the host cell.[3]

Brome mosaic virus (BMV) is a plant virus representative of a broad category of ssRNA viruses; it has proven to be a good model for virus replication studies.[4] Its capsid is composed of 180 copies of the same protein, arranged with $T = 3$ icosahedral symmetry.[5] Protein−protein interactions including electrostatic and hydrophobic are able to stabilize the BMV capsid even in the absence of RNA. Coulomb forces dominate RNA−protein interactions, speeding up assembly and adding stability to the virion. However, specific interactions also exist.[6,7] The BMV genome is divided into four segments, RNA1, RNA2, RNA3, and RNA4, packaged in morphologically identical capsids. RNA1 and RNA2 are packaged individually as single molecules, whereas RNA3 is copackaged with subgenomic RNA4. The physiochemical properties of the virions depend on the type of RNA they contain. It is believed that differences in stability are important for orchestrating RNA release.[8,9] Methods used to control virion-stabilizing interactions in vitro include changing temperature,[10] pH,[11] and ionic strength.[12,13]

Nearly all plant viruses multiply in the cytoplasm. In vitro, BMV virus particles are stable at acidic pH and low ionic strength but disassemble at basic pH in the absence of divalent cations. Intracellular pH varies from 6.0 to 7.5 and salt concentrations are below 200 mM.[14] According to the in vitro phase diagram, these conditions are too mild to result in the breakdown of BMV virions.[15] Thus, the chemical force driving disassembly must be different for the uncoating of BMV RNA in the cell,[3] or disassembly (uncoating) is not necessary in order to present the RNA to the host translational machinery. The latter scenario forms the cotranslational disassembly hypothesis,[16−18] whereby RNA presentation is mediated by a global capsid rearrangement known as the swelling transition. This feature, common in a few icosahedral plant viruses, including BMV, can be induced in vitro by increasing the pH above 6.5 and removing stabilizing divalent cations.[19,20] The capsid remains stable when fully swollen because of the ionic interactions between positively charged side groups of the coat

Received: January 1, 2020
Revised: February 20, 2020
Published: March 6, 2020

https://dx.doi.org/10.1021/acs.jpcb.0c00008
J. Phys. Chem. B 2020, 124, 2124–2131

proteins and the negatively charged polyphosphate backbone of RNA. The involvement of a swelling transition in the cotranslational hypothesis has been challenged through mutational assays for the chlorotic cowpea mottle virus (CCMV)[21]—a close relative of BMV. In this case, an alternative presentation pathway was proposed, which maintains the idea of partial protection of the RNA by a capsid that does not completely disassemble. The nature of potential disassembly intermediates is therefore central to the translational processes. Moreover, it offers potential clues for the design of virus-based gene therapy vectors.[22,23]

In vitro studies of the disassembly of empty BMV and CCMV capsids have been performed by neutron scattering,[15] time-resolved small-angle X-ray scattering (TR-SAXS),[24] and a fluorescence thermal shift assay.[25,26] Tresset and co-workers used TR-SAXS to investigate the disassembly of empty CCMV capsids triggered by a pH change from acidic to neutral conditions at 0.5 M ionic strength.[24] They observed large intermediates, small intermediates, and dimers. The large intermediates were assigned to capsids that had split into two pieces, and the smaller intermediates were assigned as fragments of the large intermediates. However, whereas neutron scattering and TR-SAXS provide average size information, unambiguous identification of intermediates is difficult because the results are averaged over many intermediates.

In this work, we use charge detection mass spectrometry (CDMS) to identify disassembly intermediates for BMV. CDMS is well suited to the analysis of high mass, heterogeneous samples.[27−40] It is a single-particle technique where the m/z and charge (z) of each ion are measured simultaneously using a detection cylinder embedded in an electrostatic linear ion trap. Measurement of both m/z and z avoids the need to resolve charge states in the m/z spectrum, which is necessary with conventional MS. The m/z and z are multiplied to give the mass of each ion and the masses are then binned to give a mass distribution. Previously, CDMS has been used to identify assembly intermediates for the hepatitis B virus (HBV) capsid[36−38] and to analyze samples of adeno-associated virus where empty particles and particles with a full genome and partial genome were resolved.[39]

In this study, we used two CDMS-based approaches to investigate the disassembly of BMV. In the first, a rapid mixing device coupled to CDMS is used to record mass distributions at fixed time points after a rapid pH change at varying salt concentrations. In the second, CDMS spectra are measured as a function of time after the addition of EDTA (ethylenediaminetetraacetic acid). EDTA chelates divalent cations and promotes swelling and disassembly of the BMV capsids at neutral pH. These studies address two pathways of in vitro virus disassembly. The pH jump is thought to weaken protein−RNA and protein−protein interactions and promote RNA release. Under these conditions, the results suggest that the BMV virions disassemble into two large fragments: a nearly complete capsid that has released the RNA and the released RNA complexed to a small number of capsid proteins. In the second pathway (where the capsid is disrupted by chelation of divalent cations), the RNA continues to interact strongly with the capsid proteins, whereas the protein−protein interactions are weakened. Under these conditions, the virion mass initially increases presumably because the RNA is exposed through the pores of the swollen capsid and able to recruit additional capsid proteins to the complex.

RESULTS

The BMV capsid protein has a molecular mass of 20,295 Da, and so the expected mass of the empty $T = 3$ capsid is 3.653 MDa. The packaged RNAs have masses of approximately 1.042, 0.921, and 0.962 MDa for RNA1, RNA2, and RNA3/4, respectively.[41] Thus, the virions should have molecular masses of 4.695, 4.574, and 4.615 MDa, respectively. The BMV virions employed in this study were derived from *Nicotiana benthamiana* (see the Methods section). The relative abundances of the RNA1, RNA2, and RNA3/4 containing virions are expected to lie in the ranges of around 9−12, 14−30, and 59−77%, respectively.[42,43] Taking into account the relative abundances and the resolution of the CDMS measurements, the three forms are expected to coalesce into a single, almost-Gaussian peak at around 4.61 MDa with a full width at half-maximum (fwhm) of around 0.136 MDa. A figure showing the coalescence of the three peaks is given in the Supporting Information (Figure S1). The instrumental resolution and the expected uncertainty in the mass measurements are discussed in the Methods section.

Native mass spectrometry requires the use of a buffer composed of a volatile salt; ammonium acetate is a widely used choice and was employed here. A typical CDMS spectrum of freshly purified BMV, buffer exchanged into 100 mM ammonium acetate at pH 5.15, is shown in Figure 1. The

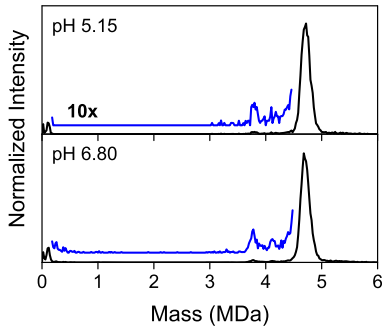

Figure 1. CDMS spectra of wt BMV in 100 mM ammonium acetate at pH 5.15 (top) and at pH 6.80 (bottom). Intensities for portions of the spectra corresponding to intermediate masses have been multiplied 10x (blue lines).

main peak at 4.71 MDa (peak width 0.194 MDa) is almost certainly due to BMV virions. When the same BMV sample is buffer exchanged into 100 mM of ammonium acetate at neutral pH (pH 6.80), the main peak position is virtually unchanged at 4.70 MDa (peak width 0.191 MDa), indicating that a pH change alone does not disassemble BMV, at least on the timescale of these experiments (where buffer exchange takes around 10 min and data collection takes around 30 min). The peaks at around 4.7 MDa were the highest mass features observed in these CDMS spectra: BMV dimers and higher-order multimers were not detected.

The peak assigned to the full BMV capsids at around 4.70 MDa is almost 2.0% larger than the expected mass of 4.61 MDa. Deviations are known to occur in native mass spectrometry of protein complexes because of incomplete desolvation, counter ions, and adduct addition. In this case, counter ions are also expected to be associated with at least some of the RNA backbone phosphate groups, which should be ionized, except under very acidic conditions. The peak at 4.70 MDa is considerably broader than expected. The

https://dx.doi.org/10.1021/acs.jpcb.0c00008
J. Phys. Chem. B 2020, 124, 2124−2131

measured fwhm is 0.194 MDa and the expected fwhm is 0.136 MDa (as discussed above). The increased peak width indicates that there is an additional source of heterogeneity, which is consistent with the measured mass being slightly higher than expected.

In addition to the main peak at around 4.70 MDa, there are small peaks at around 3.78 MDa in Figure 1. This is near to the expected mass of the empty capsid (3.653 MDa). However, the deviation is 3.6%, which seems too large for this peak to be attributed to the empty capsid. Furthermore, the empty capsid is not thought to be stable under the conditions used here.[44] Instead, we hypothesize that the peak at 3.78 MDa may correspond to almost empty BMV capsids stabilized by one or more cellular RNA fragments, or to a low abundance capsid variant with around 77% of a $T = 3$ capsid proteins. This capsid variant was not observed by other methods, perhaps because of its low abundance.

Disassembly by pH Jump. Previous work has shown that raising the ionic strength to greater than 1 M with lithium chloride at neutral pH causes BMV to disassemble.[24] Involatile salts like lithium chloride are incompatible with electrospray ionization and so we attempted to induce disassembly by raising the ammonium acetate concentration. BMV did not significantly disassemble with ammonium acetate concentrations up to 1 M, and higher concentrations interfered with the electrospray process. As an alternative to raising the ionic strength, we explored the idea of using of a pH change to cause disassembly. Raising the pH to around 10.5 was found to cause rapid disassembly of BMV with the rate of disassembly depending on the ammonium acetate concentration. MALDI (matrix-assisted laser desorption and ionization) mass spectra and gel electrophoresis assays showed that the integrities of both the protein and RNA were not affected by this pH within the experimental time frame (see Figures S2 and S3 in the Supporting Information).

To provide a short reaction time and minimize subsequent aggregation of disassembly intermediates and products, a rapid mixing device was used to introduce the BMV virions to the basic environment. The resulting mixture travels along a capillary and then the disassembly reaction is terminated by electrospraying the mixture. The reaction time can be varied by changing the length of the capillary between the mixing device and the electrospray source. The pH jump was generated by mixing a solution of BMV virions in ammonium acetate (pH of 6−7) with a solution that consisted of ammonium hydroxide and the same concentration of ammonium acetate as the BMV solution (pH around 11). The resulting mixture had a pH of 10.2−10.6, depending on the ammonium acetate concentration employed (see Table S1 in the Supporting Information for typical pHs). Several reaction times were tested. The results presented here were obtained with a reaction time of 30 s and are illustrative of the main intermediates observed.

Figure 2 shows CDMS spectra measured with ammonium acetate concentrations ranging from 75 to 10 mM. In all cases, the BMV concentration was 0.20 mg/mL after mixing. The dashed vertical line at 4.71 MDa is at the center of the peak assigned to intact BMV. With an ammonium acetate concentration of 75 mM (top spectrum in Figure 2) most of the virions remain intact. The 75 mM spectrum in Figure 2 is similar to the spectra in Figure 1. There is intensity in the 75 mM spectrum for masses below 0.2 MDa that presumably results from dimers, small dimer oligomers, and perhaps some small RNA fragments. However, 75 mM ammonium acetate at a pH of around 10.5 is apparently too mild to cause efficient capsid disassembly within 30 s.

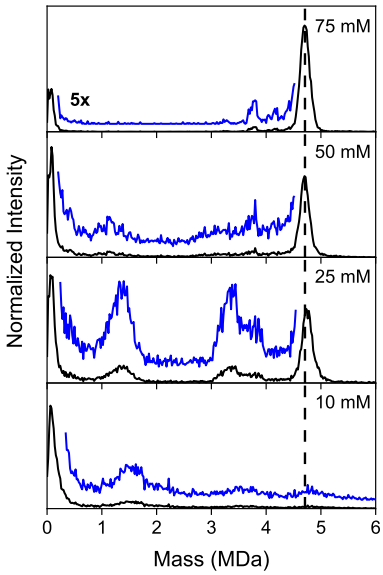

Figure 2. CDMS spectra measured for BMV disassembly induced by a pH jump with a rapid mixing device. The measurements were made (i.e., the samples were electrosprayed) 30 s after mixing. The dashed vertical line at 4.71 MDa is at the center of the peak assigned to intact BMV virions. The intermediate mass ranges are magnified 5× to show low-intensity features. Several different ammonium acetate concentrations were used, ranging from 75 to 10 mM. The ammonium acetate concentration employed in each case is indicated on the spectra. The BMV concentration after mixing was 0.2 mg/mL for all samples and the pH after mixing was 10.2−10.5, depending on the ammonium acetate concentration (see Table S1 in the Supporting Information for typical pHs). The spectra are normalized so that the most intense feature in each spectrum has approximately the same intensity.

When the ammonium acetate concentration was lowered to 50 mM (second spectrum from the top in Figure 2), there was a substantial increase in the number of ions with intermediate masses (i.e., between 0.5 and 3.5 MDa). However, the features are broad and there were no well-defined peaks present in the intermediate regime. Ions with masses below 0.5 MDa are significantly more abundant that in the 75 mM spectrum.

Upon further reduction of the ammonium acetate concentration to 25 mM, there was a substantial increase in the intensities at intermediate masses, with two broad peaks emerging, centered on around 1.42 and 3.33 MDa. In addition, there is a smaller peak centered on around 3.85 MDa that appears as a high mass shoulder on the larger 3.33 MDa peak. We attribute these features to the initial products of the disassembly process. Note that the sum of the masses of the two main peaks, 3.33 and 1.42 MDa, is very close to the mass of the BMV virion, suggesting the possibility that the virion cleaves, in one event, into two large fragments. However, it is not possible to say which fragment retains the RNA from the mass measurements alone.

In Table 1, we consider two limiting disassembly scenarios where either all the RNA is retained in one fragment or no RNA is retained. With these assumptions, we determine the fraction of capsid proteins that must be retained to give the masses of the main features in the 25 mM spectrum at 3.85, 3.33, and 1.42 MDa.

https://dx.doi.org/10.1021/acs.jpcb.0c00008
J. Phys. Chem. B 2020, 124, 2124−2131

Table 1. Fraction of the Capsid Proteins Remaining for the Three Main Peaks Observed in the CDMS Spectra Measured for Disassembly at pH ~10.5 and Low Salt

	fraction of capsid proteins remaining	
peak, MDa	all RNA retained (%)	no RNA retained (%)
3.85	79	
3.33	65	93
1.42	13	40

The peak at around 3.85 MDa must have retained at least some of the ~1 MDa RNA (because it is less than 1 MDa from the 4.71 MDa peak). If all the RNA is retained in the species responsible for the 3.85 MDa peak, only around 79% of the capsid proteins remain. For the peak at around 3.33 MDa, the fraction of the capsid proteins that remain is 65% if all the RNA is retained, and around 93% if none of the RNA is retained. Finally, for the 1.42 MDa peak, only around 13% of the capsid proteins remain if all the RNA is retained. This fraction increases to 40% if all the RNA is lost.

Finally, with 10 mM ammonium acetate (bottom spectrum in Figure 2), few intact capsids remain after 30 s. There is a broad low-intensity distribution in the CDMS spectrum that extends to masses beyond 6 MDa. The species with masses greater than 4.7 MDa presumably results from the aggregation of capsid fragments. There is a small maximum in the distribution at around 1.5 MDa, which is close to the mass of the large peak in the 25 mM spectrum. However, the peaks between 3 and 4 MDa have largely vanished, suggesting that the larger fragments undergo further dissociation to yield small fragments.

To further investigate the nature of the species formed by BMV disassembly following the pH jump, transmission electron microscopy (TEM) images were recorded for BMV capsids after a pH jump in 25 mM ammonium acetate. For the images in Figure 3A,B, the samples were applied to the grids immediately after the solutions were mixed to generate the pH jump. For the images in Figure 3C,D, the samples were applied to the grids around 15 min after mixing. For Figure 3A,B (samples applied immediately after mixing), some of the BMV virions appear to remain intact (as indicated by the black arrows in Figure 3A,B) and some appear to have broken up (white arrows). In the BMV virions that appear to be intact, a dense core can often be observed, which is usually located asymmetrically within the capsid and only partially adhering to the lumenal surface. We associate this core with a condensed form of RNA. Incomplete (broken) capsids are abundant and, significantly, they mostly appear to be empty. In Figure 3C,D (sample applied around 15 min after mixing), most of the capsids are broken into smaller fragments and some of the genome appears to be bound to a small amount of capsid protein. The red arrows indicate possible RNA density associated with capsid fragments. In both cases, the images show many capsids which have a stain that has penetrated the virus. This is indicative of disruption of the barrier quality of the virus capsid. Taken together, these results suggest that the 3.33 MDa peak in the CDMS spectra following the pH jump (Figure 2) is due to empty partial capsids and the lower mass 1.42 MDa peak is due to RNA complexed with a few capsid proteins.

Disassembly via a Swelling Transition. The second approach to virus disassembly examined here was designed to include the reversible swelling transition that is known to occur for BMV. This requires more moderate conditions that are closer to equilibrium. Swelling, a 10% expansion of the virus capsid, results from removal of Mg^{2+} cations by a chelating agent and deprotonation of glutamic acid residues above pH 6.2.[19] The swollen structure has sixty 2 nm pores[45] and the RNA becomes accessible to RNAse degradation.[20]

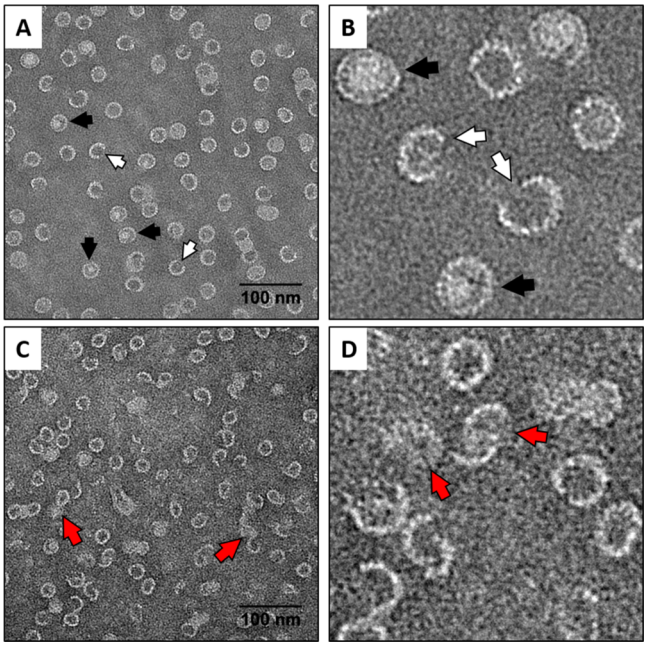

Figure 3. TEM images of negatively stained wt BMV capsids disassembled by a jump to pH ~10.5 in 25 mM ammonium acetate. (A) Image of wt BMV capsids placed on the EM grids immediately after the pH jump. Note shells with dense core (black arrows) and empty shells with small missing part (white arrows). (B) Zoomed in portion of the image in (A). (C) Image of wt BMV capsids placed on the grid 15 min after the pH jump. (D) Zoomed in portion of the image in (C). The red arrows indicate possible RNA density associated with capsid fragments.

To induce the swelling transition, BMV virions were dialyzed against an ammonium acetate solution that contained 1 nM of EDTA for varying lengths of time. CDMS mass distributions measured as a function of dialysis time are shown in Figure 4. For an ammonium acetate concentration above 75 mM, we did not observe a significant disassembly for a dialysis time of 24 h. The results presented in Figure 4 are from experiments performed with 10 mM ammonium acetate at pH 7. The BMV virions were initially transferred into a 10 mM ammonium acetate solution without EDTA by means of a buffer exchange column. The spectrum measured at time $t = 0$ (the top spectrum in Figure 4) is similar to the BVM spectra in Figure 1. The main peak at 4.74 MDa is attributed to intact BMV virions with small contributions from peaks at 3.78, 3.27 MDa, and a low mass peak at around 120 kDa. As dialysis and exposure to EDTA progresses, the mass distributions change. After 1 h, the peak attributed to the virion has broadened and shifted to a higher mass. There is also a substantial increase in the abundance of ions with masses less than 1 MDa.

After 3 h, the broadening and shift of the peak originally attributed to the virion have continued. At this point, the center of the high mass peak has shifted to a higher mass by over 0.5 MDa and the width has more than doubled. The fraction of ions with masses < 1 MDa has continued to increase and a second peak with a mass of around 500 kDa has

https://dx.doi.org/10.1021/acs.jpcb.0c00008
J. Phys. Chem. B 2020, 124, 2124−2131

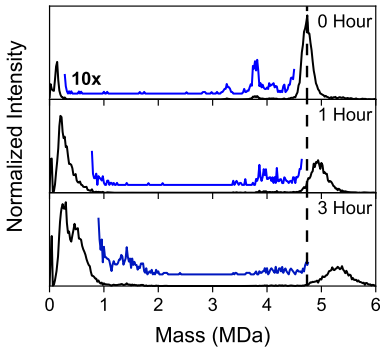

Figure 4. CDMS spectra measured as a function of time during dialysis of wt BMV into 1 nM EDTA at pH 6.8. The BMV capsid concentration was 0.2 mg/mL. The intermediate portions of each spectrum have been magnified by 10× (blue line). Spectra are shown for 0, 1, and 3 h after starting dialysis. The vertical dashed line at 4.74 MDa is at the center of the main peak in the 0 h spectrum, which is assigned to intact wt BMV.

appeared. A low-intensity distribution centered around 1.4 MDa has also appeared. This peak has a mass that is similar to the low mass peak in Figure 2 that was tentatively assigned to RNA associated with a few capsid proteins.

Figure 5 shows negative stain TEM images taken for some of the same time points as the CDMS measurements shown in Figure 4. Before dialysis (Figure 5A), most particles appear to be close to spherical. The stain has not penetrated inside the capsid very much, which suggests that the genome is distributed across the lumenal surface (see white arrow heads for examples). At the 1 h dialysis time point (Figure 5B), it appears that the stain has penetrated some of the particles (see black arrowheads for examples). With increased time of exposure to EDTA (Figure 5C,D), the particles appear less spherical and the number of broken particles increases. In the image from the 3 h time point (Figure 5D), most particles are broken and many shaded unstructured areas are observed, which may consist of nucleoprotein complexes (examples are indicated by white arrows).

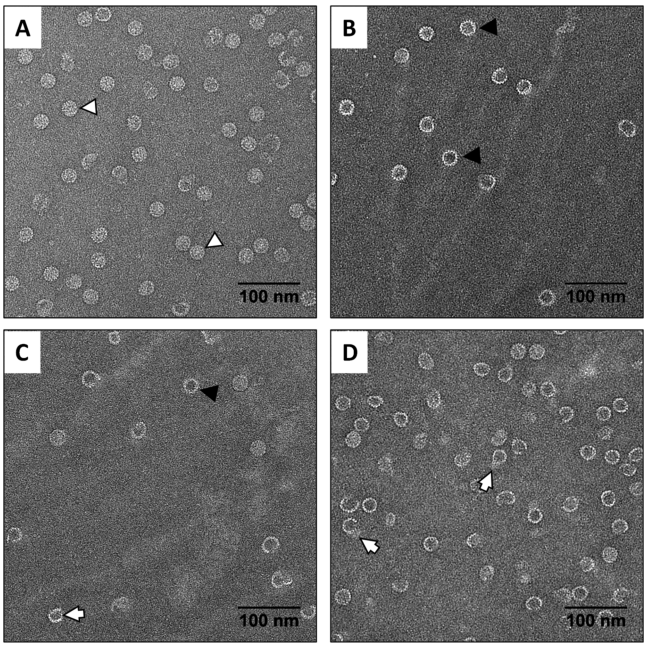

Figure 5. TEM images of wild-type (wt) BMV virions disassembled under moderate conditions. (A) Image of wt BMV virions in 100 mM ammonium acetate at pH 7. (B–D) Images of wt BMV particles in 100 mM ammonium acetate at pH 7 after 1, 2, and 3 h dialysis with 1 nM EDTA. Note: stain does not penetrate inside the capsid before dialysis (white arrowhead), after dialysis the stain has penetrated most capsids (black arrowhead), at the longer time points some density is visible outside the capsids (white arrows).

DISCUSSION

In the case of the pH jump experiments, our results suggest that disassembly is mainly driven by a disruption of the normal interactions between the RNA and the capsid proteins. EM images show that at close to neutral pH, the RNA is distributed over the lumenal cavity wall. At high pH, the RNA collapses to form an often asymmetrically disposed dense core, suggesting that the RNA has condensed. It is known that RNA condensation can be caused by ammonium ions replacing water around the RNA and providing a bridge between RNA strands by hydrogen bonding with phosphate oxygens.[46] In addition, the pH is slightly above pI = 10.7 for free arginine. Arginine is a major component of the N-termini of BMV coat proteins involved in electrostatic interactions with the genome.[47]

The weakening of genome–capsid interactions allows for the formation of two main disassembly products attributed to a near complete capsid without the genome and the free genome with a small number of capsid proteins attached. This cleavage may occur through the propagation of a crack that separates the nucleoprotein complex from a partial empty shell.

Interestingly, crack propagation through an avalanche mechanism has been observed in recent rapid compression experiments by atomic force microscopy.[48] In that work, empty capsids had a lower barrier for crack propagation than virions. Preliminary simulations consistent with the experimental results suggested that capsid failure occurs through dislocation proliferation, which supports the idea of cleavage of empty partial capsids. This disassembly pathway closely resembles the one proposed previously to explain early experiments done at high LiCl salt concentration and neutral pH.[15]

The second disassembly pathway examined here involves weakening of capsid protein–protein interactions by removal of magnesium cations, which are known to stabilize the capsid.[5,19] The magnesium ions were removed by chelation with EDTA. As the magnesium ions are removed from the virus capsid at neutral pH, the carboxyl groups of glutamic acid residues at the protein–protein interfaces become deprotonated, causing a repulsion between the proteins. The capsid swells by around 10% and pores, ∼2 nm in diameter, form at the threefold symmetry axes.[43] In this case, the interactions between the capsid proteins and RNA are not substantially altered. However, it has been shown that capsid structural transitions are accompanied by RNA rearrangement.[10,49] Specifically, RNA expands radially toward the surface of the particle as the capsid swells. The opening of pores in the virus capsid exposes the RNA to solution, which allows the RNA to bind capsid proteins from solution. The binding of additional capsid proteins causes the mass of the particle to increase. As shown in Figure 4, the mass of the main peak in the CDMS spectra systematically increases with dialysis time. Under these conditions, the capsid proteins are not stripped from the genome and this pathway of swelling and capsid disruption matches the cotranslational disassembly model proposed by

https://dx.doi.org/10.1021/acs.jpcb.0c00008
J. Phys. Chem. B 2020, 124, 2124–2131

Wilson et al.,[16,50] where the coat proteins continue to protect the RNA from the environment, while at the same time allowing host machinery to bind to RNA to begin transcription. Thus, when the BMV capsid swells and the coat protein lattice is disrupted, it is possible that the RNA does not need to leave the capsid to be exposed to the cellular organelles to start replication.

CONCLUSIONS

Two distinct pathways of BMV capsid disassembly have been discovered by CDMS and TEM. When a pH jump rapidly places the virions into a basic environment, they mainly break through a global cleavage event into two fragments attributed to a near complete capsid that has released the RNA and a nucleoprotein fragment consisting of the released RNA complexed to a small number of the capsid proteins. The empty capsid subsequently breaks apart into smaller fragments. This behavior is similar to what is observed under high ionic strength conditions where the RNA is released leaving behind an almost complete empty capsid.

Upon slow buffer exchange and removal of divalent cations the protein−protein interactions are disrupted and the BMV capsids swell. However, there is no evidence for separation of the RNA from the capsid, indicating that solution conditions which disrupt the coat protein interactions alone are not sufficient to strip the capsid protein from the genome. In this case, the peak attributed to the virion increases in mass with time, suggesting that additional proteins associate with the exposed RNA in the disrupted coat protein−RNA complex. It is likely that this pathway is more closely related to how the capsid disassembles in vivo, as it offers the advantage of protecting the RNA with coat protein until translation begins.

METHODS

Preparation of BMV Capsids. Solutions were prepared with ultrapure water (18 MΩ cm at 25 °C) and analytical grade reagents. All reagents, unless specified, were purchased from Sigma-Aldrich (St Louis, MO) and used as received. BMV was expressed in *N. benthamiana* via Agrobacterium-mediated gene delivery.[51] Seven days after infection, *N. benthamiana* leaves were homogenized in virus buffer (250 mM NaOAc, 10 mM $MgCl_2$, at pH 4.5) and then centrifuged at 5,000 rpm for 25 min using an Eppendorf F-35-6-30 rotor. The supernatant was layered on a 10% sucrose cushion in virus buffer and centrifuged at 26,000 rpm for 3 h using a Beckman SW 32 rotor. The pellets were re-suspended in 38.5% CsCl (w/v, virus buffer) and centrifuged at 45,000 rpm for 24 h on a Beckman 65 TY rotor. The resulting virus band was collected and dialyzed against SAMA buffer [50 mM NaOAc, 8 mM $Mg(OAc)_2$, at pH 4.6] for 24 h, with three changes. The virus concentration was measured by UV−vis absorption spectrometry using a NanoDrop 1000 at 260 nm [$\varepsilon A(0.1\%) = 5.15$]. For CDMS, the BMV samples were transferred into ammonium acetate solutions of specified concentration by spin-column SEC (Bio-Rad Laboratories, Inc.).

Transmission Electron Microscopy. Electron-transparent samples were prepared by placing 10 μL of a dilute sample onto a carbon-coated copper grid. After 10 min, the excess solution on the grid was removed with filter paper. Samples were stained with 10 μL of NanoVan (methylamine vanadate, at pH 8) for 10 min. The excess solution was removed by blotting with filter paper and the sample was then left to dry for several minutes. Images were acquired at an accelerating voltage of 120 kV on a JEOL JEM 1400 plus transmission electron microscope and analyzed with the ImageJ Processing Toolkit to estimate the diameters of the particles.

CDMS Interfaced with a Rapid Mixing Device. Measurements were performed on a home-built instrument described elsewhere.[52−56] CDMS is a single-particle technique where the m/z (mass to charge ratio) and charge are simultaneously determined for individual ions and then the m/z and charge are multiplied to give the mass. Measurements are performed for several thousand ions and then binned to give a mass spectrum.

Ions are generated by a commercial nESI source (Advion Triversa Nanomate) operated in positive mode, and enter the CDMS instrument through a heated capillary. The ions pass through an ion funnel, an RF hexapole ,and an RF quadrupole. They are then accelerated through a potential difference of 100 V and focused into a dual hemispherical deflection analyzer (HDA). The HDA transmits a narrow band of kinetic energies into the ion trap where ions are trapped and oscillate back and forth through a detection cylinder. The ion trap is a modified cone trap and the detection cylinder is embedded between the two ends caps. With the end caps grounded, ions pass through the trap. The first step in a trapping cycle is to raise the potentials on the back end cap to the trapping potential. Ions are then deflected back through the trap. Shortly after, the potential on the front end cap is raised to the trapping potential. Ions in the trap when the front end cap is switched to trapping mode are trapped and oscillate back and forth through the detection cylinder. When ions enter the detection cylinder, they induce a charge which is detected by a charge sensitive amplifier; when they leave the induced charge dissipates. After a predetermined trapping time (100 ms in these experiments), the end caps are set to ground to empty the trap.

The periodic signal from the trapped ion is amplified, digitized, and then analyzed in real time by a Fortran program using fast Fourier transforms. The ion signal was optimized to maximize the fraction of single ion trapping events. Empty, partial (where an ion is trapped for less than 100 ms), and multiple ion trapping events were discarded during data analysis. The m/z is derived from the oscillation frequency and the charge is derived from the magnitudes of the fundamental and first harmonic. The calibration of the charge and m/z measurements has been described elsewhere.[54] Before binning, the ions were weighted by $m/z^{-1/2}$ to compensate for the trapping probability being inversely proportional to the ion velocity.

The mass resolving power is determined by the precision of the m/z and charge measurements. The precision of the charge measurement is determined mainly by the trapping time. With the 100 ms trapping time used here, the RMSD in the charge measurement is around 1.2e (elementary charges). The precision of the m/z measurements is limited mainly by the energy distribution of the ions. The ion energy affects the ion's oscillation frequency. Under the conditions used here the m/z resolving power is around 50. Combining the m/z resolving power with the z resolving power (around 64) leads to a mass resolving power for the BMV virion of around 39. The expected peak width (fwhm) for a single homogeneous species with a mass of 4.6 MDa is around 117 kDa. The accuracy of the mass measurement depends on the calibration of the m/z and charge measurements. The calibration is performed using

https://dx.doi.org/10.1021/acs.jpcb.0c00008
J. Phys. Chem. B 2020, 124, 2124−2131

pyruvate kinase (PK). PK is a tetramer in solution and under native electrospray conditions the mass spectrum for PK contains the tetramer and multimers of the tetramer (i.e., octamer, dodecamer, etc.). We have previously shown that charge states can be resolved for PK with long trapping times. The absolute uncertainty in the mass measurements is estimated to be ±25 kDa.

In order to monitor the BMV disassembly reaction at specific time points, a rapid mixing device was interfaced with the commercial nano-electrospray source. The rapid mixing device included a dual syringe pump that had one syringe loaded with intact BMV capsids in ammonium acetate at a neutral pH and the other syringe was loaded with the same concentration of ammonium acetate, but at a pH value of around 11. When the two solutions were mixed, the BMV concentration is halved, the ammonium acetate concentration is unchanged, and the pH becomes around 10.9−11.0. A total flow rate (after mixing) of 500 nL/min was employed. The syringes were connected to a PEEK mixing tee (P-888 from IDEX Health & Science) by fused silica capillaries (Polymicro Technologies, 363 μm O.D.). The flow exits the mixing tee via a fused silica capillary with a cross-sectional area larger than the combined cross-sectional areas of the two capillaries entering the mixing tee. The inner diameter of the exiting capillary is stepped down with a P-720 microtight union assembly (IDEX Health & Science) to match the inner diameter of the Advion LC Coupler, which allows the rapid mixing setup to be interfaced with the chip-based nESI source (Advion Triversa Nanomate). The length of the capillary exiting the mixing tee dictates the reaction time. The reaction time can be estimated from the flow rate and the volume of the exiting capillary. A variety of reaction times were employed. Results shown here were obtained with a reaction time of 30 s.

■ ASSOCIATED CONTENT

Supporting Information

The Supporting Information is available free of charge at https://pubs.acs.org/doi/10.1021/acs.jpcb.0c00008.

Coalescence of peaks with different RNA contents, a MALDI spectrum showing the integrity of the capsid protein, gel electrophoresis of the extracted RNA showing the integrity of RNA, and pH values after mixing (PDF)

■ AUTHOR INFORMATION

Corresponding Authors

Bogdan Dragnea − *Chemistry Department, Indiana University, Bloomington, Indiana 47405, United States;* orcid.org/0000-0003-0611-2006; Email: dragnea@iu.edu

Martin F. Jarrold − *Chemistry Department, Indiana University, Bloomington, Indiana 47405, United States;* orcid.org/0000-0001-7084-176X; Email: mfj@iu.edu

Authors

Kevin M. Bond − *Chemistry Department, Indiana University, Bloomington, Indiana 47405, United States*

Nicholas A. Lyktey − *Chemistry Department, Indiana University, Bloomington, Indiana 47405, United States*

Irina B. Tsvetkova − *Chemistry Department, Indiana University, Bloomington, Indiana 47405, United States*

Complete contact information is available at: https://pubs.acs.org/10.1021/acs.jpcb.0c00008

Author Contributions

†K.M.B. and N.A.L. contributed equally.

Notes

The authors declare the following competing financial interest(s): The authors except MFJ declare no competing financial interest. MFJ is associated with a company that is developing charge detection mass spectrometry.

■ ACKNOWLEDGMENTS

This material is based upon work supported by the National Science Foundation under grant number CHE-1531823 (to M.F.J.) and CBET-1740432 (to B.D.).

■ REFERENCES

(1) Gelderblom, H. R. Structure and Classification of Viruses. In *Medical Microbiology*; Baron, S., Ed.; The University of Texas Medical Branch at Galveston: Galveston, Texas, 1996.

(2) Mandahar, C. L. Infection by and uncoating of virus particles. In *Multiplication of RNA Plant Viruses*; Mandahar, C. L., Ed.; Springer Netherlands: Dordrecht, The Netherlands, 2006.

(3) Greber, U. F.; Singh, I.; Helenius, A. Mechanisms of Virus Uncoating. *Trends Microbiol.* **1994**, *2*, 52−56.

(4) Kao, C. C.; Sivakumaran, K. Brome Mosaic Virus, Good for an RNA Virologist's Basic Needs. *Mol. Plant Pathol.* **2000**, *1*, 91−97.

(5) Lucas, R. W.; Larson, S. B.; McPherson, A. The Crystallographic Structure of Brome Mosaic Virus. *J. Mol. Biol.* **2002**, *317*, 95−108.

(6) Choi, Y. G.; Grantham, G. L.; Rao, A. L. N. Molecular Studies on Bromovirus Capsid Protein. *Virology* **2000**, *270*, 377−385.

(7) Wang, Z.; Hryc, C. F.; Bammes, B.; Afonine, P. V.; Jakana, J.; Chen, D.-H.; Liu, X.; Baker, M. L.; Kao, C.; Ludtke, S. J.; Schmid, M. F.; Adams, P. D.; Chiu, W. An Atomic Model of Brome Mosaic Virus Using Direct Electron Detection and Real-Space Optimization. *Nat. Commun.* **2014**, *5*, 4808.

(8) Hoover, H. S.; Wang, J. C.-Y.; Middleton, S.; Ni, P.; Zlotnick, A.; Vaughan, R. C.; Kao, C. C. Phosphorylation of the Brome Mosaic Virus Capsid Regulates the Timing of Viral Infection. *J. Virol.* **2016**, *90*, 7748−7760.

(9) Vaughan, R.; Tragesser, B.; Ni, P.; Ma, X.; Dragnea, B.; Kao, C. C. The Tripartite Virions of the Brome Mosaic Virus Have Distinct Physical Properties That Affect the Timing of the Infection Process. *J. Virol.* **2014**, *88*, 6483−6491.

(10) Incardona, N. L.; McKee, S.; Flanegan, J. B. Noncovalent Interactions in Viruses: Characterization of their Role in the pH and Thermally Induced Conformational Changes in Bromegrass Mosaic Virus. *Virology* **1973**, *53*, 204−214.

(11) Hiebert, E.; Bancroft, J. B.; Bracker, C. E. The Assembly In Vitro of Some Small Spherical Viruses, Hybrid Viruses, and Other Nucleoproteins. *Virology* **1968**, *34*, 492−508.

(12) Yamazaki, H.; Kaesberg, P. Degradation of Bromegrass Mosaic Virus with Calcium Chloride and the Isolation of its Protein and Nucleic Acid. *J. Mol. Biol.* **1963**, *7*, 760−762.

(13) Cuillel, M.; Zulauf, M.; Jacrot, B. Self-assembly of brome mosaic virus protein into capsids. *J. Mol. Biol.* **1983**, *164*, 589−603.

(14) Martinière, A.; Bassil, E.; Jublanc, E.; Alcon, C.; Reguera, M.; Sentenac, H.; Blumwald, E.; Paris, N. In Vivo Intracellular pH Measurements in Tobacco and Arabidopsis Reveal an Unexpected pH Gradient in the Endomembrane System. *Plant Cell* **2003**, *25*, 4028−4043.

(15) Cuillel, M.; Berthetcolominas, C.; Timmins, P. A.; Zulauf, M. Reassembly of Brome Mosaic-Virus from Dissociated Virus - A Neutron-Scattering Study. *Eur. Biophys. J.* **1987**, *15*, 169−176.

(16) Brisco, M.; Hull, R.; Wilson, T. M. A. Swelling of Isometric and of Bacilliform Plant Virus Nucleocapsids Is Required for Virus-Specific Protein Synthesis in Vitro. *Virology* **1986**, *148*, 210−217.

(17) Roenhorst, J. W.; van Lent, J. W. M.; Verduin, B. J. M. Binding of Cowpea Chlorotic Mottle Virus to Cowpea Protoplasts and

Relation of Binding to Virus Entry and Infection. *Virology* **1988**, *164*, 91−98.
(18) Roenhorst, J. W.; Verduin, B. J. M.; Goldbach, R. W. Virus-Ribosome Complexes from Cell-Free Translation Systems Supplemented with Cowpea Chlorotic Mottle Virus Particles. *Virology* **1989**, *168*, 138−146.
(19) Incardona, N. L.; Kaesberg, P. A pH-Induced Structural Change in Bromegrass Mosaic Virus. *Biophys. J.* **1964**, *4*, 11−21.
(20) Liepold, L. O.; Revis, J.; Allen, M.; Oltrogge, L.; Young, M.; Douglas, T. Structural Transitions in Cowpea Chlorotic Mottle Virus (CCMV). *Phys. Biol.* **2005**, *2*, S166−S172.
(21) Albert, F. G.; Fox, J. M.; Young, M. J. Virion Swelling Is Not Required for Cotranslational Disassembly of Cowpea Chlorotic Mottle Virus in Vitro. *J. Virol.* **1997**, *71*, 4296−4299.
(22) Azizgolshani, O.; Garmann, R. F.; Cadena-Nava, R.; Knobler, C. M.; Gelbart, W. M. Reconstituted Plant Viral Capsids Can Release Genes to Mammalian Cells. *Virology* **2013**, *441*, 12−17.
(23) Lam, P.; Steinmetz, N. F. Delivery of SiRNA Therapeutics Using Cowpea Chlorotic Mottle Virus-like Particles. *Biomater. Sci.* **2019**, *7*, 3138−3142.
(24) Law-Hine, D.; Sahoo, A. K.; Bailleux, V.; Zeghal, M.; Prevost, S.; Maiti, P. K.; Bressanelli, S.; Constantin, D.; Tresset, G. Reconstruction of the Disassembly Pathway of an Icosahedral Viral Capsid and Shape Determination of Two Successive Intermediates. *J. Phys. Chem. Lett.* **2015**, *6*, 3471−3476.
(25) Tresset, G.; Chen, J.; Chevreuil, M.; Nhiri, N.; Jacquet, E.; Lansac, Y. Two-Dimensional Phase Transition of Viral Capsid Gives Insights into Subunit Interactions. *Phys. Rev. Appl.* **2017**, *7*, 014005.
(26) Chen, J.; Chevreuil, M.; Combet, S.; Lansac, Y.; Tresset, G. Investigating the Thermal Dissociation of Viral Capsid by Lattice Model. *J. Phys. Condens. Matter* **2017**, *29*, 474001.
(27) Fuerstenau, S. D.; Benner, W. H. Molecular Weight Determination of Megadalton-DNA Electrospray Ions Using Charge Detection Mass Spectrometry. *Rapid Commun. Mass Spectrom.* **1995**, *9*, 1528−1538.
(28) Benner, W. H. A Gated Electrostatic Ion Trap to Repetitiously Measure the Charge and *m/z* of Large Electrospray Ions. *Anal. Chem.* **1997**, *69*, 4162−4168.
(29) Fuerstenau, S. D.; Benner, W. H.; Thomas, J. J.; Brugidou, C.; Bothner, B.; Siuzdak, G. Mass Spectrometry of an Intact Virus. *Angew. Chem. Int. Ed.* **2001**, *113*, 559−562.
(30) Mabbett, S. R.; Zilch, L. W.; Maze, J. T.; Smith, J. W.; Jarrold, M. F. Pulsed acceleration charge detection mass spectrometry: Application to Weighing Electrosprayed Droplets. *Anal. Chem.* **2007**, *79*, 8431−8439.
(31) Doussineau, T.; Kerleroux, M.; Dagany, X.; Clavier, C.; Barbaire, M.; Maurelli, J.; Antoine, R.; Dugourd, P. Charging Megadalton Poly(ethylene oxide)s by Electrospray Ionization. A Charge Detection Mass Spectrometry Study. *Rapid Commun. Mass Spectrom.* **2011**, *25*, 617−623.
(32) Doussineau, T.; Désert, A.; Lambert, O.; Taveau, J.-C.; Lansalot, M.; Dugourd, P.; Bourgeat-Lami, E.; Ravaine, S.; Duguet, E.; Antoine, R. Charge Detection Mass Spectrometry for the Characterization of Mass and Surface Area of Composite Nanoparticles. *J. Phys. Chem. C* **2015**, *119*, 10844−10849.
(33) Doussineau, T.; Mathevon, C.; Altamura, L.; Vendrely, C.; Dugourd, P.; Forge, V.; Antoine, R. Mass Determination of Entire Amyloid Fibrils by Using Mass Spectrometry. *Angew. Chem. Int. Ed.* **2016**, *55*, 2340−2344.
(34) Elliot, A. G.; Harper, C. C.; Lin, H.-W.; Williams, E. R. Mass, Mobility and MS^n Measurements of Single Ions Using Charge Detection Mass Spectrometry. *Analyst* **2017**, *142*, 2760−2769.
(35) Elliott, A. G.; Harper, C. C.; Lin, H.-W.; Susa, A. C.; Xia, Z.; Williams, E. R. Simultaneous Measurements of Mass and Collisional Cross-Section of Single Ions with Charge Detection Mass Spectrometry. *Anal. Chem.* **2017**, *89*, 7701−7708.
(36) Pierson, E. E.; Keifer, D. Z.; Selzer, L.; Lee, L. S.; Contino, N. C.; Wang, J. C.-Y.; Zlotnick, A.; Jarrold, M. F. Detection of Late Intermediates in Virus Capsid Assembly by Charge Detection Mass Spectrometry. *J. Am. Chem. Soc.* **2014**, *136*, 3536−3541.
(37) Lutomski, C. A.; Lyktey, N. A.; Zhao, Z.; Pierson, E. E.; Zlotnick, A.; Jarrold, M. F. HBV Capsid Completion Occurs Through Error Correction. *J. Am. Chem. Soc.* **2017**, *139*, 16932−16938.
(38) Lutomski, C. A.; Lyktey, N. A.; Pierson, E. E.; Zhao, Z.; Zlotnick, A.; Jarrold, M. F. Multiple Pathways in Capsid Assembly. *J. Am. Chem. Soc.* **2018**, *140*, 5784−5790.
(39) Pierson, E. E.; Keifer, D. Z.; Asokan, A.; Jarrold, M. F. Resolving Adeno-Associated Viral Particle Diversity with Charge Detection Mass Spectrometry. *Anal. Chem.* **2016**, *88*, 6718−6725.
(40) Dunbar, C. A.; Callaway, H. M.; Parrish, C. R.; Jarrold, M. F. Probing Antibody Binding to Canine Parvovirus with Charge Detection Mass Spectrometry. *J. Am. Chem. Soc.* **2018**, *140*, 15701−15711.
(41) Ahlquist, P. Bromovirus RNA Replication and Transcription. *Curr. Opin. Genet. Dev.* **1992**, *2*, 71−76.
(42) Ni, P.; Vaughan, R. C.; Tragesser, B.; Hoover, H.; Kao, C. C. The Plant Host Can Affect the Encapsidation of Brome Mosaic Virus (BMV) RNA: BMV Virions Are Surprisingly Heterogeneous. *J. Mol. Biol.* **2014**, *426*, 1061−1076.
(43) Chakravarty, A.; Reddy, V. S.; Rao, A. L. N. Unravelling the Stability and Capsid Dynamics of the Three Virions of Brome Mosaic Virus Assembled Autonomously In Vivo. *J. Virol.* **2020**, DOI: 10.1128/JVI.01794-19, accepted manuscript.
(44) Pfeiffer, P.; Hirth, L. Aggregation States of Brome Mosaic Virus Protein. *Virology* **1974**, *61*, 160−167.
(45) Speir, J. A.; Munshi, S.; Wang, G.; Baker, T. S.; Johnson, J. E. Structures of the Native and Swollen Forms of Cowpea Chlorotic Mottle Virus Determined by X-Ray Crystallography and Cryo-Electron Microscopy. *Structure* **1995**, *3*, 63−78.
(46) Pesavento, J. B.; Lawton, J. A.; Estes, M. K.; Prasad, B. V. V. The Reversible Condensation and Expansion of the Rotavirus Genome. *Proc. Natl. Acad. Sci. U.S.A.* **2001**, *98*, 1381−1386.
(47) Ni, P.; Wang, Z.; Ma, X.; Das, N. C.; Sokol, P.; Chiu, W.; Dragnea, B.; Hagan, M.; Kao, C. C. An Examination of the Electrostatic Interactions between the N-Terminal Tail of the Brome Mosaic Virus Coat Protein and Encapsidated RNAs. *J. Mol. Biol.* **2012**, *419*, 284−300.
(48) Hernando-Pérez, M.; Zeng, C.; Miguel, M. C.; Dragnea, B. Intermittency of Deformation and the Elastic Limit of an Icosahedral Virus under Compression. *ACS Nano* **2019**, *13*, 7842−7849.
(49) Jacrot, B. Studies on the Assembly of a Spherical Plant Virus. II. The Mechanism of Protein Aggregation and Virus Swelling. *J. Mol. Biol.* **1975**, *95*, 433−446.
(50) Shields, S. A.; Brisco, M. J.; Wilson, T. M. A.; Hull, R. Southern Bean Mosaic Virus RNA Remains Associated with Swollen Virions during Translation in Wheat Germ Cell-Free Extracts. *Virology* **1989**, *171*, 602−606.
(51) Gopinath, K.; Kao, C. C. Replication-Independent Long-Distance Trafficking by Viral RNAs in Nicotiana Benthamiana. *Plant Cell* **2007**, *19*, 1179−1191.
(52) Contino, N. C.; Jarrold, M. F. Charge Detection Mass Spectrometry for Single Ions with a Limit of Detection of 30 Charges. *Int. J. Mass Spectrom.* **2013**, *345-347*, 153−159.
(53) Contino, N. C.; Pierson, E. E.; Keifer, D. Z.; Jarrold, M. F. Charge Detection Mass Spectrometry with Resolved Charge States. *J. Am. Soc. Mass Spectrom.* **2013**, *24*, 101−108.
(54) Pierson, E. E.; Keifer, D. Z.; Contino, N. C.; Jarrold, M. F. Probing Higher Order Multimers of Pyruvate Kinase with Charge Detection Mass Spectrometry. *J. Mass Spectrom.* **2013**, *337*, 50−56.
(55) Pierson, E. E.; Contino, N. C.; Keifer, D. Z.; Jarrold, M. F. Charge Detection Mass Spectrometry for Single Ions with an Uncertainty in the Charge Measurement of 0.65 e. *J. Am. Soc. Mass Spectrom.* **2015**, *26*, 1213−1220.
(56) Keifer, D. Z.; Shinholt, D. L.; Jarrold, M. F. Charge Detection Mass Spectrometry with Almost Perfect Charge Accuracy. *Anal. Chem.* **2015**, *87*, 10330−10337.

https://dx.doi.org/10.1021/acs.jpcb.0c00008
J. Phys. Chem. B 2020, 124, 2124−2131